ISSN: 3007-9640 DOI: https://doi.org/10.70114/acmsr.2025.5.1.P122

Validation of ISAA-Na Code for Sodium-Cooled Fast Reactors: CABRI-BI1, AGS0, and E7 Experiments

Shaowei Tang [1, a] *, Bin Zhang [1,2, b]

[1] School of Nuclear Science and Technology, Xi'an Jiaotong University, Xi'an, Shaanxi, China;

[2] State Key Laboratory of Multiphase Flow in Power Engineering, Xi'an Jiaotong University, Xi'an, Shaanxi, China.

[a] tangshaowei@stu.xjtu.edu.cn, [b] binzhang@mail.xjtu.edu.cn

Abstract. Accurate transient behavior modeling is crucial for assessing the safety of sodium-cooled fast reactors (SFRs) . This study validates the ISAA-Na code through simulations of the CABRI-BI1, AGS0, and E7 experiments. The CABRI-BI1 experiment, focused on sodium boiling, was simulated using a multi-bubble slug flow model. Results showed that ISAA-Na more accurately predicted coolant temperature and pressure prior to boiling than SAS4A, ASTEC-Na, and SIMMER. In the CABRI-E7 experiment, ISAA-Na's cladding failure model was tested under transient overpower (TOP) conditions. ISAA-Na's results closely matched experimental data and other codes, successfully predicting fission gas release, coolant temperature, and cladding failure timing and location. The CABRI-AGS0 experiment further examined fuel pin behavior under TOP conditions. ISAA-Na accurately captured fission gas release, temperature, and fuel melting radius predictions. Overall, ISAA-Na demonstrates strong potential for SFR transient analysis, though further refinement in phase transition modeling is needed. This validation provides valuable insights into ISAA-Na's capability to enhance SFR safety assessments.

Keywords: Sodium-cooled fast reactors; ISAA-Na ; Two-phase flow; CABRI experiment

1. Introduction

Sodium-cooled fast reactors (SFRs) possess excellent thermal-hydraulic properties and are considered one of the advanced reactor types in the fourth generation of nuclear reactors. According to China's "three-step" development strategy for thermal reactors, fast reactors, and fusion reactors, the development of fast reac-tors, exemplified by SFRs, plays a critical role in addressing China's energy challenges[1]. As the develop-ment of sodium-cooled fast reactors progresses, there is an urgent need to develop new methods and employ advanced computational tools and techniques to analyze the safety and severe accident scenarios of these reactors.

In the past, due to limitations in computer performance and insufficient understanding of the complex coupled phenomena during accidents, computational analysis of SFRs mainly focused on mechanistic codes and specialized codes. To meet China's future needs for safety analysis of sodium-cooled fast reactors, a version of the Integrated Severe Accident Analysis code (ISAA[2]) tailored for SFRs, known as ISAA-Na, is currently under development. The development plan for ISAA-Na includes reactivity effect model, thermal-hydraulic model, fuel pin thermo-mechanical model, core melt migration model, debris bed cooling model, and sodium fire model.

CABRI was an international research program in which the French IRSN (formerly IPSN), the French CEA , the German KIT (formerly KFK), the British UKAEA, the North Americans US/DOE and the US/NRC and the Japanese JAEA (formerly PNC) participated[3]. In this study, three different experimental tests (BI1, AGS0, and E7) conducted in the CABRI experimental facility were selected. The ISAA-Na code was used to model and simulate these experiments, and the computational results were compared with the experimental data and the results from other sodium-cooled fast reactor analysis codes to validate the accu-racy of the models implemented in ISAA-Na.

ISSN: 3007-9640 DOI: https://doi.org/10.70114/acmsr.2025.5.1.P122

2. Physics Models of ISAA-Na

2.1 Thermal-Hydraulic Model

ISAA-Na simulates the entire reactor core by dividing it into multiple radial rings. Within each radial ring, a channel modeling approach is employed, and different node schemes are applied to each channel as needed to meet the requirements for sodium-cooled fast reactor accident analysis. Each channel represents a fuel pin, its associated coolant, and a portion of the subassembly duct wall.

The thermal-hydraulic calculations for the reactor core in ISAA-Na are performed within the aforemen-tioned framework. A large number of sodium boiling experimental results indicate that during boiling, a small bubble initially forms within the channel, and this bubble continues to grow, leaving a liquid film on the cladding and structures. As the fuel pin temperature increases, additional bubbles may form at other locations. These bubbles either burst or merge, growing into larger bubbles. When the wall dries out, the cladding directly exchanges heat with the steam. Based on these phenomena, ISAA-Na adopts a multi-bubble slug boiling model, as shown in Figure 1.

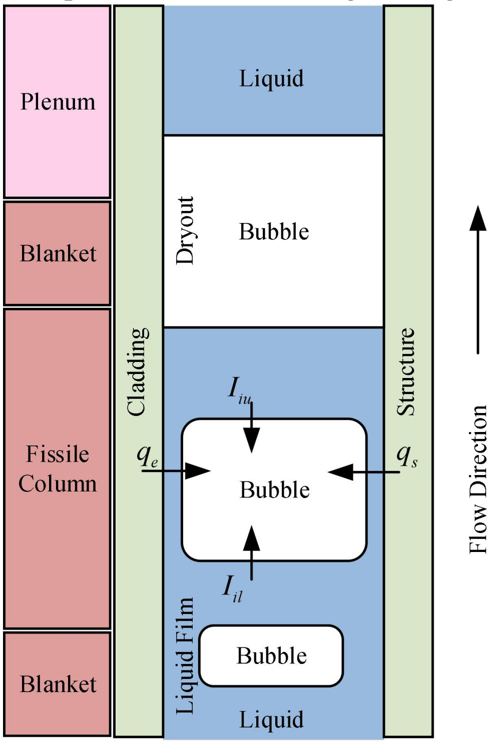

Fig. 1 Schematic diagram of multi-bubble slug boiling model

Before boiling, the coolant in the entire channel is treated as a liquid slug, and the temperature and pres-sure of each grid in the slug are calculated. When the temperature of the coolant in a given grid exceeds the saturation temperature by 10 K, boiling is considered to begin, marking the initial condition for bubble for-mation [4]. If the length of the bubble is smaller than the grid length or the set minimum length, the bubble is considered a small bubble, and it is assumed that the vapor pressure inside the bubble is uniformly distrib-uted, treating the vapor as a whole. Otherwise, if the bubble length exceeds the grid length, it is considered a large bubble, where a vapor pressure gradient exists within the bubble, and the thermodynamic parameters of the vapor phase differ across different grids. The liquid between bubbles is treated as a liquid slug. Ignor-ing the inlet and outlet conditions, the coolant in the single-phase state within the channel can be regarded as a whole, forming a large liquid slug. The two-phase liquid slugs and the large liquid slug in the single-phase state are treated with the same heat transfer and flow equations.

ISSN: 3007-9640 DOI: https://doi.org/10.70114/acmsr.2025.5.1.P122

2.2 Fuel Pin Thermo-Mechanical Model

A fuel pin thermo-mechanical model, which comprehensively considers various effects during irradiation and transient periods, has been developed for ISAA-Na[5] and has been validated through experiments. This model is divided into fuel-pin mechanics and fuel-pin phenomenology. The mechanistic model includes calculations of axial and radial strains, thermoelastic stresses, and axial expanding of fuel and cladding. The phenomenological model considers phenomena such as porosity, grain wroth, irradiation-induced cladding swelling, fuel-cladding gap conductance, fission product swelling, fission-gas generation and release, fuel-cladding interaction, and fuel restructuring.

2.3 Cladding Failure Model

As described above, a fuel pin thermo-mechanical model has been developed for ISAA-Na. To account for multiple factors that could lead to cladding failure under various accident scenarios in SFRs, ISAA-Na in-corporates a cladding failure model that includes multiple failure mechanisms. Different empirical relation-ships are used for each failure mode, and the failure time and location of the cladding are determined based on various calculated parameters. These relationships primarily stem from previous related experiments and are also used in other sodium-cooled fast reactor analysis codes. In ISAA-Na, the thermodynamic model of the fuel rod calculates parameters such as temperature, stress, and strain at each node of the fuel pin, provid-ing input for the cladding failure model. Once cladding failure occurs, the disappearance of certain nodes influences the thermodynamic model of the fuel pin, and the interaction between the two models is shown in Figure 2.

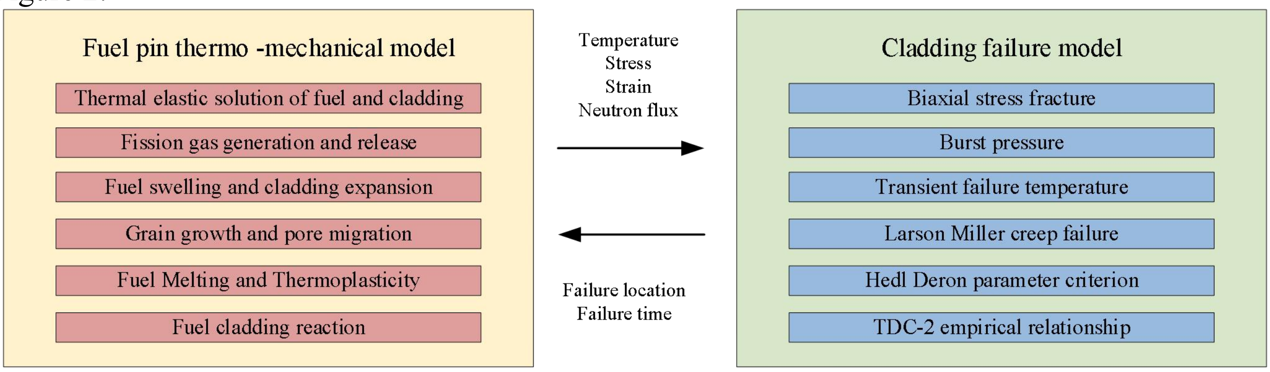

Fig. 2 The relationship between the fuel pin thermo-mechanical model and cladding failure model of ISAA-Na

This cladding failure model primarily considers six failure criteria, including biaxial stress fracture, burst pressure, transient failure temperature, Larson-Miller creep failure, Hedl-Dorn parameter criterion, and the TDC-2 empirical relationship. A detailed description of these models can be found in reference[6].

3. BI1 test

3.1 Initial And Boundary Conditions

The BI1 test was a loss of flow experiment conducted using the CABIR experimental facility, employing mixed oxide test fuel pin irradiated in the PHENIX reactor, with a maximum burnup of 1 at.%. During the experiment, steady-state conditions were first reached by achieving a peak linear power of 662 W/cm. Sub-sequently, the coolant inlet flow rate was gradually reduced from 0s, while maintaining constant power, until the coolant in the channel began to boil at around 20s. As the bubbles increased, the two-phase inter-face extended upwards and downwards. At

ISSN: 3007-9640 DOI: https://doi.org/10.70114/acmsr.2025.5.1.P122
approximately 25.8 seconds, the cladding failed, causing fuel melting and ejecting into the channel. The reactor was then shut down, and the experiment was terminated around 30 seconds.

The fuel pin parameters for the BI1 test are shown in Table 1, and the initial and boundary conditions are provided in Table 2. These parameters are derived from the reference[7].

Table 1. Characteristics of RIG-1 fuel pins

Parameter	Value
Cladding outer diameter[mm]	7.605
Cladding inner diameter[mm]	6.565
Cladding material	316-CW
Pellet diameter[mm]	6.4
Fissile column length [mm]	748.8
Upper axial blanket length [mm]	99.5
Lower axial blanket length [mm]	200.2
Peak burnup[at.%]	1.0
Pin length[mm]	1500.5
Upper fission gas plenum length [cm]	9.4

Table 2. Initial and boundary conditions for the CABRI-BI1 experiment

Parameter	Value
Power produced in the test section[W]	37120.0
Fissile power[W]	36230.0
Test channel inlet mass flow rate[kg/s]	0.161±3%
Temperature at BFC[K]	676±0.3%
Temperature at TFC[K]	859±0.3%
Sodium pressure at outlet[bar]	2.43

3.2 Calculation Results And Analysis

The simulation of the CABRI-BI1 experiment is divided into steady-state and transient phases. The objec-tive of the steady-state calculation is to replicate the experimental conditions before the start of the transi-ent. The calculations are performed based on the steady-state boundary conditions provided in Table 2, with the results shown in Fig. 3 and Fig. 4. In the figures, alongside the ISAA-Na calculation results, the results from SIMMER, ASTEC-Na, and SAS4A are also presented. These results are sourced from the reference[7].

Fig. 3 shows a comparison of the steady-state coolant pressure and cladding temperature, where the re-sults from the four codes are in close agreement. Fig. 4 illustrates the steady-state axial coolant temperature distribution. In the fissile region, the temperature increases predicted by all four codes are very close to the experimental results. However, in the temperature plateau above the blanket, only the ISAA-Na and SAS4A simulations accurately match the experimental data.

ISSN: 3007-9640 DOI: https://doi.org/10.70114/acmsr.2025.5.1.P122

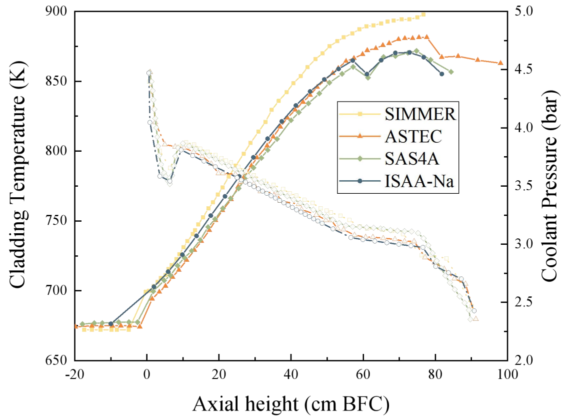

Fig. 3 Axial profile of the coolant pressure and cladding temperature at steady state conditions

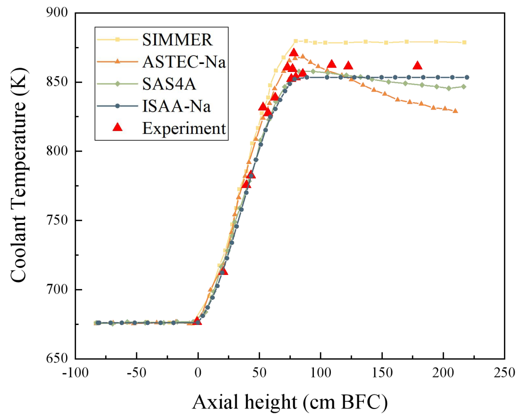

Fig. 4 Axial profile of the coolant pressure and cladding temperature at steady state conditions

Fig. 5 show comparisons of the inlet coolant flow rates, with the flow rate being expressed as volumetric flow. The experimental section begins boiling at around 20 seconds, after which the inlet flow rate starts oscillating at around 22 seconds. All four codes accurately predict the onset of boiling.

The axial coolant temperature distribution before boiling is shown in Fig. 6. Among the results from the four codes, only ISAA-Na accurately predicts both the coolant temperature peak and the temperature distri-bution in the upper part of the fissile region. SIMMER calculates a coolant temperature that is higher than the experimental values, while SAS4A and ASTEC-Na predict temperatures that are lower than the experi-mental data.

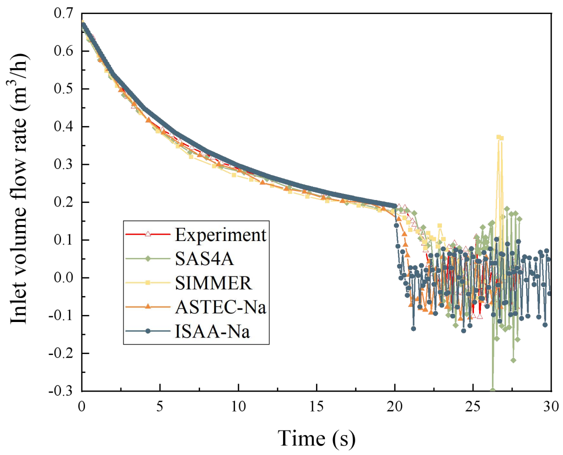

Fig. 5 Inlet flow rate during the transient

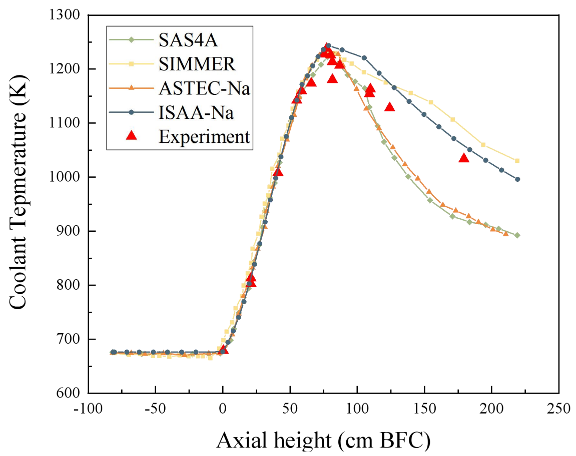

Fig. 6 Axial coolant temperature at t =20s

Fig. 7 shows the variation of the two-phase interface in the BI1test, with TC (Thermo Couple) represent-ing the measurements from the thermocouples and VD (Void Detector) representing the measurements from the void detectors. The two-phase interface calculated by the codes refers to the highest and lowest interface of the bubbles in the channel

ISSN: 3007-9640 DOI: https://doi.org/10.70114/acmsr.2025.5.1.P122

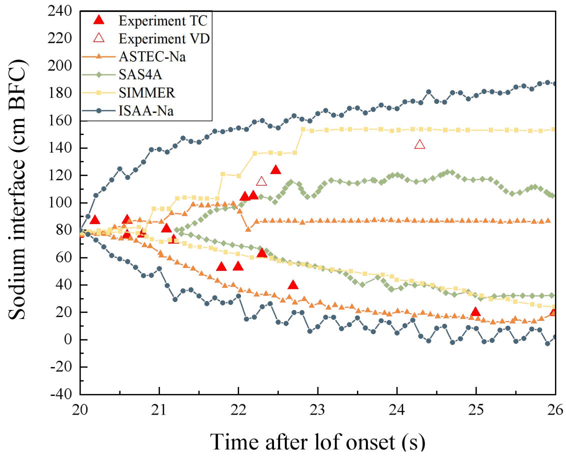

Fig. 7 Sodium two-phase interface during BI1 test

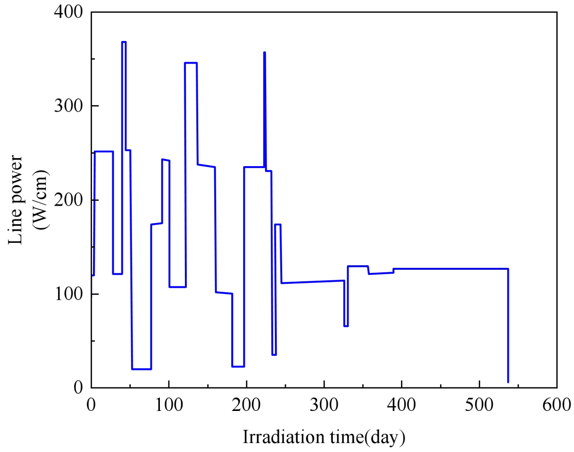

Fig. 8 Power histories for the RIG-2 fuel pin

4. AGS0 Test

4.1 Initial And Boundary Conditions

AGS0 test is a structured transient over-power test conducted under standard cooling conditions[8][9], using the RIG-2 fuel pin that had been irradiated in a PFR reactor. The fuel pin contains a solid fuel pellet, but after irradiation in the reactor, it develops a central hole (with a maximum diameter of 1 mm). The cladding material is 316 CW stainless steel. During the AGS0 experiment, the over-power conditions did not lead to cladding failure, but partial melting occurred inside the fuel pin. The purpose of this experiment was to assess the melting of the fuel rod and the release of fission gases under transient over-power conditions.

Fig. 8 shows the irradiation history of the RIG-2 fuel pin. Fig. 9 presents the transient power variation in the AGS0 test, with the maximum power reaching 12 times the standard power, and the peak occurring at approximately 0.4 seconds.

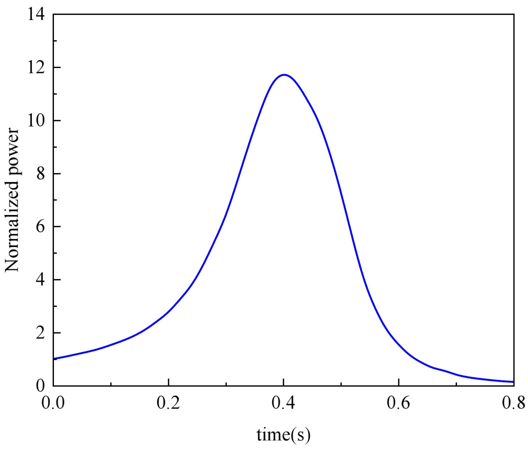

Fig. 9 Normalized transient power for AGS0 test

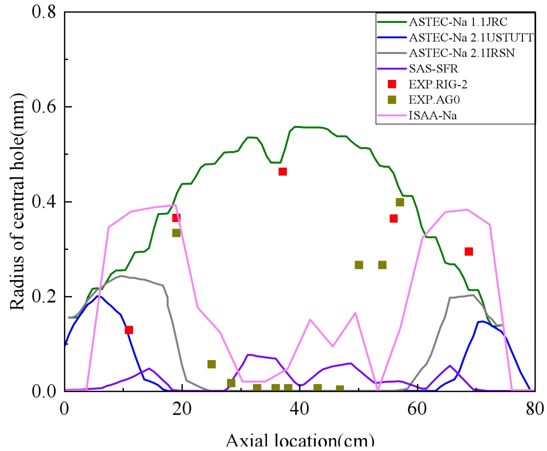

Fig. 10 Calculated fuel central hole radius at t = 0s

4.2 Calculation Results And Analysis

At t = 0s, the radius of the fuel pin central hole is shown in Fig. 10. In this figure, the results from five dif-ferent simulation codes are presented, along with the central hole radius after pre-irradiation (EXP RIG-2) and the radius after thermal calibration in the AG0 experiment. The AG0 experiment was conducted in the CABRI experimental facility and used the same RIG-2 fuel pin, so the data from the thermal calibration in the AG0 experiment is assumed to be nearly

ISSN: 3007-9640 DOI: https://doi.org/10.70114/acmsr.2025.5.1.P122

identical to that of the AGS0 experiment. The results indicate that, except for ASTEC-Na V1.1, all other codes are able to reproduce the phenomenon of the central hole closure in the fuel pin after thermal calibration.

Fig. 11 shows the axial coolant temperature distribution at t = 0s. The calculated results from the six codes are in good agreement with the experimental values. Fig. 12 shows the axial coolant temperature distribution at t = 0.8s. Multiple experimental values are pro-vided at the same axial positions because thermocouples were arranged at different orientations in the CABRI facility. Due to the inherent asymmetry of the fuel pin or other uncertainties, slight variations in temperature readings were observed from the thermocouples positioned at different angles.

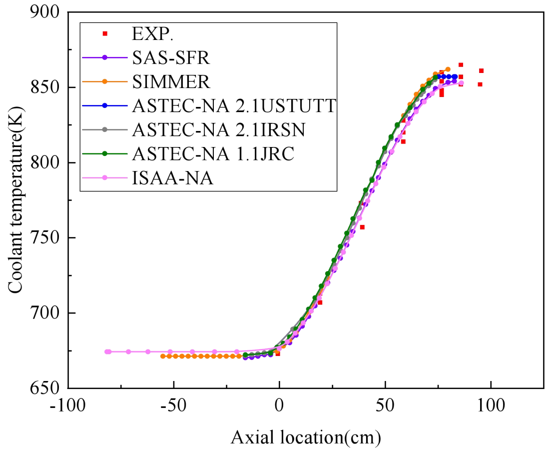

Fig. 11 Coolant temperature axial profile at t = 0s

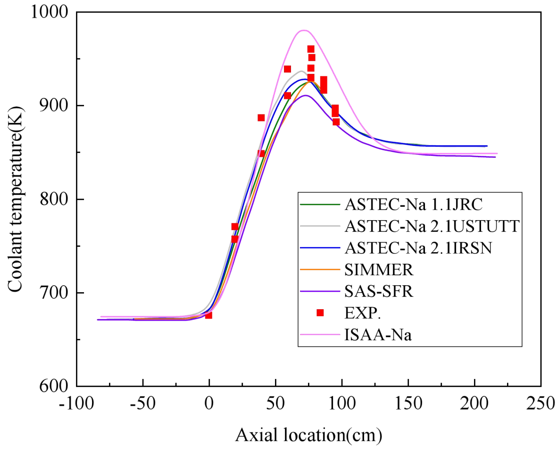

Fig. 12 Coolant temperature axial profile at t = 0.8s

Fig. 13 shows the fission gas retention at different axial positions of the fuel pin. Three sets of measure-ment values are included in the figure. The PIE (Post Irradiation Examination) represents the measurements taken after irradiation and serves as the reference. The AGS0 values correspond to the steady-state meas-urements after the AGS0 experiment, which are used for comparison with the simulation results at t = 0s. The PTE (Post-Test Examination) values represent the measurements taken after the test, which are used for comparison with the simulation results at t = 1.5s.

The measured centerline melting range of the fuel rod after the experiment is shown in Fig. 14. The axial position of the melting ranges from approximately 20 cm to 60 cm, with a maximum melting radius of 1.2 mm. From the figure, it can be observed that the melting ranges predicted by the five programs differ slight-ly from the experimental measurements. The ISAA-Na calculation predicts a smaller melting range, approx-imately 25 cm to 55 cm, but the calculated melting radius is generally accurate.

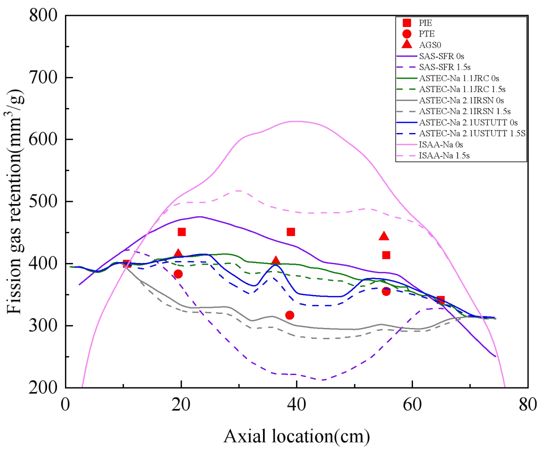

Fig. 13 Fission gas retention

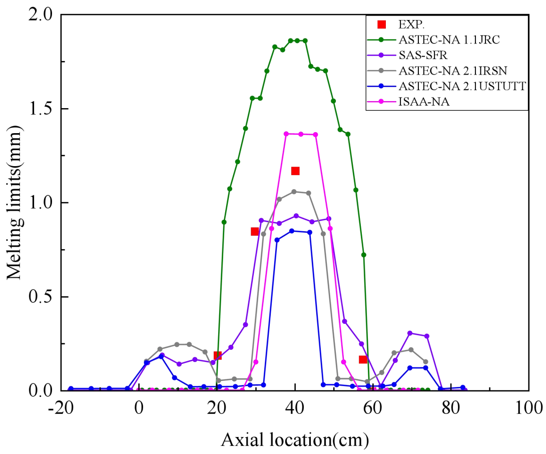

Fig. 14 Maximal radial fuel melting limits

ISSN: 3007-9640 DOI: https://doi.org/10.70114/acmsr.2025.5.1.P122

5. E7 Test

5.1 Initial And Boundary Conditions

The E7 test is a transient overpower test designed to investigate cladding failure and post-failure phenomena under transient overpower conditions, particularly the interactions between the fuel and the coolant[9]. The experiment used the Ophelie-6 annular fuel pins, which had been irradiated for over 400 days in the Phenix reactor[10]. The peak linear power in the reactor was 30.6 kW·m-1, and the maximum burnup was 4.89 at%.

After the fuel pin was transferred into the experimental apparatus, steady-state tuning began. Once steady-state conditions were achieved, a transient overpower experiment with a total duration of 1 second was conducted. The power pulse was initiated at 410 ms, reaching the maximum power pulse at 461 ms, approximately 154 times the steady-state power. During the power ramp-up, the fuel pin's interior initially melted, with the central region of the fuel nearly completely molten. Shortly after, cladding failure occurred at 467 ms, with the failure position located at a height of 53 cm. Finally, under the pressure differential between the inside and outside of the pin, the molten fuel was ejected into the coolant channel, marking the end of the experiment.

5.2 Calculation Results And Analysis

The temperature distribution of the coolant channel at steady state is shown in Fig. 15, and the temperature distribution of ISAA-Na is in good agreement with the experimental measurements. The calculation was performed based on the power variation curve provided in Fig. 16. Fig. 17 shows the axial coolant temperature distribution at t = 0.4 s, representing the experimental state prior to the arrival of the power pulse. The calculated results from all four codes are consistent with the temperature distribution curve measured by the thermocouples.

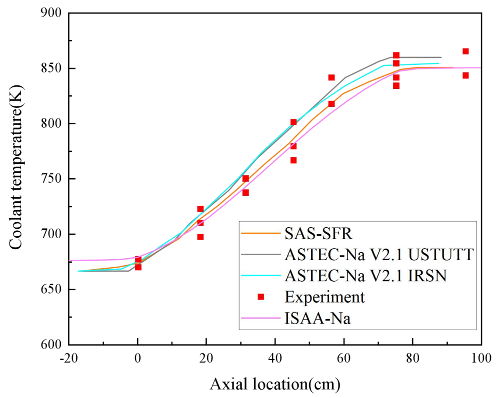

Fig. 15 Coolant temperature profile at t = 0 s

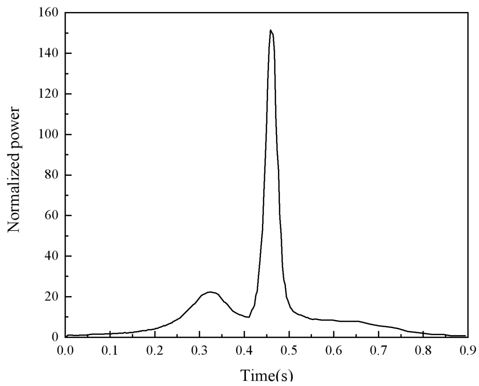

Fig. 16 Normalized power in CABRI-E7 test

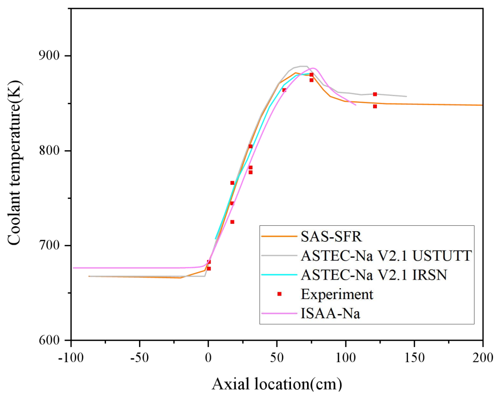

Fig. 17 Coolant temperature profile at t = 0.4 s

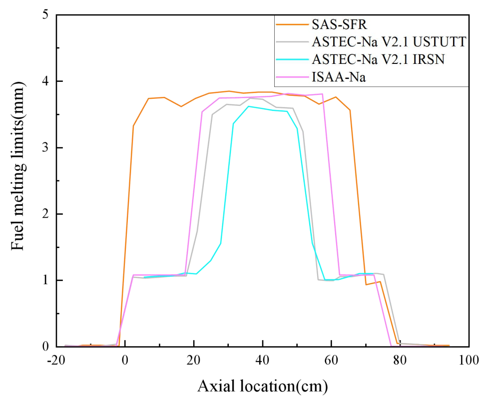

Fig. 18 Radial fuel melting limits at end time E7 test

ISSN: 3007-9640 DOI: https://doi.org/10.70114/acmsr.2025.5.1.P122

Table 3 presents the experimentally measured cladding failure time and location, along with the calcula-tion results from the four codes. The failure time predicted by ISAA-Na is 446 ms, which differs from the experimental value by 21 ms. The failure location occurs at 46.9 cm, with a difference of 6.1 cm from the experimental value. The failure is caused by reaching the transient failure temperature. Among the results from the four programs, the calculation from SAS-SFR is in the best agreement with the experimental val-ues, while the predictions from ASTEC-Na and ISAA-Na show certain discrepancies with the experimental values.

Table 2. Time and location of cladding failure

Parameter	Experiment	Astec-Na V2.1 USTUTT	Astec-Na V2.1 IRSN	SAS-SFR	ISAA-Na
Time(ms)	467	444	449	468	446
Location(cm)	53	41.3	39.4	47.7	46.9

Fig. 18 presents a comparison of the fuel melting limits predicted by the four codes. The maximum fuel melting limits predicted by all four codes reaches the fuel outer diameter, and the overall shape of the mol-ten core is similar. However, the fuel melting range predicted by SAS-SFR is the largest. As shown in Fig. 19, compared to SAS-SFR, the fuel ejection mass predicted by ISAA-Na is closer to the experimental value, although there is still some discrepancy with the experimental results.

6. Conclusions

In the simulation of the BI1 test, by comparing the results from ISAA-Na with the experimental data and the calculations from other codes, it was found that ISAA-Na provides accurate predictions for the boiling initiation time and location, as well as the coolant temperature and pressure before boiling. However, the prediction of the movement of the two-phase interface after boiling is not very accurate.

The calculation results of the AGS0 test using ISAA-Na indicate that the fuel pin thermo-mechanical model in ISAA-Na is suitable for transient over-power calculations in sodium-cooled fast reactors where no cladding failure occurs. Compared to some of the mainstream international sodium-cooled fast reactor anal-ysis codes, ISAA-Na shows higher calculation accuracy and precision.

In the prediction of cladding failure for the E7 test, ISAA-Na calculates the failure time to be 446 ms, which is 21 ms different from the experimental value. The failure location is predicted to occur at 46.9 cm, with a difference of 6.1 cm from the experimental result. The cause of failure is attributed to reaching the transient failure temperature. Among the results from the four programs, SAS-SFR shows the best agree-ment with the experimental data, but the calculation results from ISAA-Na are generally reliable.

In the above three tests, some of the parameters calculated by ISAA-Na do not closely match the experi-mental values. However, in future development work, improvements will be made to the relevant models. Overall, ISAA-Na has performed well in simulating these experiments, and the reliability of the program has been validated.

References

[1] SU Gang. (2016). The “three steps development strategy” of China nuclear power science and technology. Science & Technology Review, 34(15). https://doi.org/10.3981/j.issn.1000-7857.2016.15.002

[2] Gao, P., Zhang, B., Li, J., Tang, S., & Shan, J. (2021). Development of mechanistic cladding rupture model for integrated severe accident code ISAA. Part I: Module verification and application in CAP1400. Annals of Nuclear Energy, 158, 108305. https://doi.org/10.1016/j.anucene.2021.108305

ISSN: 3007-9640 DOI: https://doi.org/10.70114/acmsr.2025.5.1.P122
[3] Perez-Martin, S., Bandini, G., Matuzas, V., Buck, M., & Girault, N. (2015). ICONE23-2041 FIRST ANALYSIS OF AGS0, LT2 AND E9 CABRI TESTS WITH THE NEW SFR SAFETY CODE ASTEC-NA. The Proceedings of the International Conference on Nuclear Engineering (ICONE), 2015.23(0), _ICONE23-2-_ICONE23-2. https://doi.org/10.1299/jsmeicone.2015.23._icone23-2_17

[4] Schlechtendahl, E. G. (1970). Theoretical investigations on sodium boiling in fast reactors. Nuclear Science and Engineering, 41(1), 99-114.

[5] Tang, S., Lei, Y., Yang, H., Feng, S., Zhang, B., & Shan, J. (2024). Numerical Investigation of SUPERFACT-1 Experiment by a MOX fuel Pin Thermo-mechanical Model. Nuclear Engineering and Technology. https://doi.org/10.1016/j.net.2024.06.042

[6] Tang, S., Zhang, B., Feng, S. (2024), Analysis of CABRI-E7 Transient Overpower Experiment based on ISAA-Na. The Fourth Academic Annual Conference of the Nuclear Reactor Thermodynamics Branch of the Chinese Nuclear Society.

[7] Flores y Flores, A., Matuzas, V., Perez-Martin, S., Bandini, G., Ederli, S., Ammirabile, L., & Pfrang, W. (2016). Analysis of ASTEC-Na capabilities for simulating a loss of flow CABRI experiment. Annals of Nuclear Energy, 94, 175–188. https://doi.org/10.1016/j.anucene.2016.02.032

[8] Perez-Martin, S., Bandini, G., Matuzas, V., Buck, M., & Girault, N. (2015). ICONE23-2041 FIRST ANALYSIS OF AGS0, LT2 AND E9 CABRI TESTS WITH THE NEW SFR SAFETY CODE ASTEC-NA. The Proceedings of the International Conference on Nuclear Engineering (ICONE), 2015.23(0), _ICONE23-2-_ICONE23-2. https://doi.org/10.1299/jsmeicone.2015.23._icone23-2_17

[9] Perez-Martin, S., Pfrang, W., Girault, N., Cloarec, L., Laborde, L., Buck, M., Matuzas, V., Flores y Flores, A., Raison, P., Smith, A. L., Mozzani, N., Feria, F., Herranz, L., & Farges, B. (2018). Development and assessment of ASTEC-Na fuel pin thermo-mechanical models performed in the European JASMIN project. Annals of Nuclear Energy, 119, 454–473. https://doi.org/10.1016/j.anucene.2017.12.061

[10] Fukano, Y., Onoda, Y., Sato, I., & Charpenel, J. (2009). Fuel pin behavior under slow-ramp-type transient-overpower conditions in the CABRI-FAST experiments. Journal of nuclear science and technology, 46(11), 1049-1058